Biomaterials 150 (2018) 137–149

Contents lists available at ScienceDirect

Biomaterials

journal homepage: www.elsevier.com/locate/biomaterials

Surface functionalized exosomes as targeted drug delivery vehicles for cerebral ischemia therapy

Tian Tian [a, b], Hui-Xin Zhang [a], Chun-Peng He [c], Song Fan [d], Yan-Liang Zhu [c], Cui Qi [a], Ning-Ping Huang [c], Zhong-Dang Xiao [c], Zu-Hong Lu [c], Bakhos A. Tannous [b], Jun Gao [a, *]

[a] Department of Neurobiology, Key Laboratory of Human Functional Genomics of Jiangsu, Nanjing Medical University, Nanjing, Jiangsu 211166, China
[b] Experimental Therapeutics and Molecular Imaging Lab, Department of Neurology, Massachusetts General Hospital and Harvard Medical School, Boston, MA 02129, United States
[c] State Key Laboratory of Bioelectronics, School of Biological Science and Medical Engineering, Southeast University, Nanjing, Jiangsu 210096, China
[d] Department of Oral & Maxillofacial Surgery, Sun Yat-sen Memorial Hospital, Sun Yat-sen University, Guangzhou, Guangdong 510120, China

ARTICLE INFO

Article history:
Received 19 June 2017
Received in revised form
2 October 2017
Accepted 3 October 2017
Available online 4 October 2017

Keywords:
Exosomes
Drug delivery
Cerebral ischemia
Curcumin

ABSTRACT

The safe and effective delivery of drugs is a major obstacle in the treatment of ischemic stroke. Exosomes hold great promise as an endogenous drug delivery nanosystem for the treatment of cerebral ischemia given their unique properties, including low immunogenicity, innate stability, high delivery efficiency, and ability to cross the blood-brain barrier (BBB). However, exosome insufficient targeting capability limits their clinical applications. In this study, the c(RGDyK) peptide has been conjugated to the exosome surface by an easy, rapid, and bio-orthogonal chemistry. In the transient middle cerebral artery occlusion (MCAO) mice model, The engineered c(RGDyK)-conjugated exosomes (cRGD-Exo) target the lesion region of the ischemic brain after intravenous administration. Furthermore, curcumin has been loaded onto the cRGD-Exo, and administration of these exosomes has resulted in a strong suppression of the inflammatory response and cellular apoptosis in the lesion region. The results suggest a targeting delivery vehicle for ischemic brain based on exosomes and provide a strategy for the rapid and large-scale production of functionalized exosomes.

1. Introduction

Stroke is the leading cause of death and acquired disability worldwide, and ischemic stroke, induced by a thromboembolic occlusion of the cerebral artery, accounts for over 80% of all strokes [1,2]. To date, the only approved treatment for this type of stroke is recanalization *via* the application of recombinant tissue plasminogen activator (rt-PA) [1,3]. However, this approach is limited by a narrow therapeutic window (<4.5 h) and severe risk factors [4]. Many successful pharmacotherapy including various chemicals, peptides and genetic therapies that have been evaluated in experimental animal models are impeded by challenges in delivery to ischemic brain [5,6]. Hence, a safe and efficient delivery system is a critical need for therapy in the ischemic brain.

Exosomes are 40- to 150-nm extracellular vesicles (EVs) of endosomal origin and are secreted by all cell types [7,8]. As natural carriers that package bioactive molecules, various proteins, and coding and noncoding RNAs, they transfer information between cells and tissues [9,10]. In the past decade, exosomes have emerged as novel therapeutic effectors in immune therapy, regenerative medicine and drug delivery [11,12]. They are characterized by several favorable features, such as low immunogenicity, biodegradability, low toxicity, encapsulating endogenous bioactive molecules, strong protection for cargo and the ability to cross the blood-brain barrier (BBB) [13–16]. However, recent biodistribution studies of unmodified exosomes after intravenous injection revealed a rapid accumulation of exosomes in organs of the reticuloendothelial system (RES), such as the liver and spleen, and very few exosomes were delivered to the brain after systemic administration [17,18]. Thus, their targeting characteristics require improvement before exosomes can be used to deliver therapies against stroke.

The targeting ability of exosomes can be improved by surface modifications [16,19]. Recently, the popular method is the “cell

* Corresponding author. Department of Neurobiology, Nanjing Medical University, 101 Longmian Avenue, Jiangning District, Nanjing 211166, China
E-mail address: gaojun@njmu.edu.cn (J. Gao).

https://doi.org/10.1016/j.biomaterials.2017.10.012
0142-9612/

engineering" technique, wherein donor cells are engineered to produce ligand-conjugated or drug-loaded exosomes [20–22]. These cell engineering processes are complex, high-cost, and most important cannot be readily applied to pre-isolated exosomes or exosomes from body fluids [16,19]. An exciting opportunity is translating nanoparticle techniques to exosome engineering, wherein exosomes are directly modified by biochemical conjugation or hydrophobic insertion. Several previous reports demonstrated chemical reactions can be applied to exosome conjugation [23–25]. However, they are proof-of-principle experiments and lack of *in vivo* conformation. Furthermore, few studies have modified exosomes with targeting ligands for ischemic stroke.

Here, we propose an easy, rapid and efficient method to conjugate functional ligands onto exosomal surfaces using bioorthogonal copper-free azide alkyne cyclo-addition (click chemistry). The cyclo(Arg-Gly-Asp-D-Tyr-Lys) peptide [c(RGDyK)], which exhibits high affinity to integrin $\alpha_v\beta_3$ in reactive cerebral vascular endothelial cells after ischemia specifically [26–29], was conjugated on mesenchymal stromal cell (MSC)-derived exosomes surface by our method. To generate an animal model of stroke, mice were subjected to middle cerebral artery occlusion (MCAO) and reperfusion (MCAO/R). Subsequently, c(RGDyK)-conjugated exosomes (cRGD-Exo) were intravenously administered through the tail vein. Near-infrared fluorescence (NIRF) imaging and immunofluorescence showed that cRGD-Exo targeted the lesion region of the ischemic brain and entered microglia, neurons and astrocytes. Furthermore, curcumin, a natural polyphenol from *Curcuma longa*, was loaded onto the cRGD-Exo. After the administration of cRGD-Exo containing curcumin (cRGD-Exo-cur), pro-inflammatory cytokines and activated microglia were detected. The resulting data showed that cRGD-Exo-cur suppressed the inflammatory response and cellular apoptosis in the lesion region more effectively than did curcumin or exosomes treatment alone. Also, cRGD-Exo was indicated to be a targeting delivery vehicle for ischemic brain.

2. Materials and methods

2.1. Mice and cerebral ischemia model

Eight-week-old male C57BL/6 mice were supplied by the Animal Core Facility of Nanjing Medical University (Nanjing, China). All animal experiments were carried out in compliance with institutional guidelines and were approved by the Animal Care and Use Committee of Nanjing Medical University (No. IACUC-1601160). Transient focal cerebral ischemia was induced by MCAO. After the induction of anesthesia, the right MCA was occluded by inserting a 6–0 nylon monofilament suture into the right internal carotid artery. The body temperature was sustained at 37 °C with a heated blanket throughout the procedure. Successful occlusion was assured by laser Doppler flowmetry (75–90% blood flow decrease in the MCA territory). One hour after occlusion, reperfusion was allowed by suture removal. In the sham group, an identical surgical procedure was performed without disturbing the arteries.

2.2. Cell culture

Bone marrow-derived MSCs were isolated from the tibias and femurs of mice and cultured in α-minimal essential medium (α-MEM) supplemented with 10% fetal bovine serum (FBS). The human glioblastoma cell line U87 and cervical carcinoma cell line HeLa were obtained from the Type Culture Collection of the Chinese Academy of Sciences (Shanghai, China). U87 cells expressing green fluorescent protein (U87-GFP) was purchased from Obio Technology Corp. (Shanghai, China). The three cell lines were cultured in Dulbecco's modified Eagle's medium (DMEM) containing 10% FBS. All media and reagents for cell culture were purchased from Gibco (Carlsbad, CA, USA), and all cells were incubated at 37 °C in 5% CO_2.

2.3. Exosome isolation

α-MEM containing 20% FBS was centrifuged at 200,000 g for 18 h to deplete exosomes. MSCs from passages 4–6 were cultured with 10% exosome-depleted FBS for exosome production. Every 1.5–2 × 10^6 MSCs was cultured in a 100-mm dish for 48 h and 10 mL supernatant were collected. Then exosomes were isolated from the harvested supernatant according to a previous study [30]. Briefly, the supernatant was centrifuged at 300 g for 10 min, 1200 g for 20 min, and 10,000 g for 30 min at 4 °C to remove cells and debris and then filtered using a 0.22-μm filter (Millipore, Billerica, MA, USA). The filtrate was centrifuged at 140,000 g for 90 min at 4 °C in a Type Ti70 rotor using an L-80XP ultracentrifuge (Beckman Coulter, Brea, CA, USA). The exosome pellet was resuspended in PBS and ultracentrifuged again at 140,000 g for 90 min. Subsequently, the pelleted exosomes were resuspended in PBS and analyzed using a Micro BCA Protein Assay kit (Pierce, Rockford, IL, USA). To detect exosome markers and negative marker, Western blotting was carried out with anti-Alix, anti-TSG101, and anti-Calnexin antibodies (Abcam, Cambridge, UK).

2.4. Conjugation of ligands to exosomes

Reactive dibenzylcyclootyne (DBCO) groups were incorporated in amine-containing molecules on exosomes using a heterobifunctional crosslinker. Specifically, 3 μM dibenzocyclooctyne-sulfo-*N*-hydroxysuccinimidyl ester (DBCO-sulfo-NHS) (Sigma, St. Louis, MO, USA) was added to 0.5 mg/mL exosomes in PBS and allowed to react on a rotating mixer at room temperature (RT) for 4 h. Unconjugated DBCO-sulfo-NHS was removed by four washing steps on 100-kDa ultrafiltration tubes (Millipore). The DBCO-conjugated exosomes (DBCO-Exo) were then ready for linkage to azide-containing molecules *via* copper-free click chemistry. c(RGDyK) and scrambled c(RDGyK) peptide with an azide group on the lysine were synthesized by SciLight Biotechnology Co. (Beijing, China). According to the manufacturer, azide groups were introduced by conjugating 5-azidopentanoic acid to the side chain of lysine. Cy5.5 azide was purchased from Lumiprobe Co. (Hallandale Beach, FL, USA). Specifically, 0.3 μM c(RGDyK) or scrambled c(RDGyK) peptide with azide was added to DBCO-Exo in PBS, and 0.3 μM Cy5.5 azide was subsequently added if needed. The reaction was conducted on a rotating mixer at 4 °C for 12 h. All reactions were performed at pH 7.4. Then, the exosomes were floated on a 30% sucrose/D_2O cushion and centrifuged at 164,000 g for 90 min using an SW41Ti rotor (Beckman Coulter) to remove unincorporated ligands. After washing with PBS, the modified exosomes were resuspended and stored at −80 °C prior to use. To assess the successful conjugation of exosomes and azide ligands, Cy5.5-conjugated exosomes were stained by DiI, applied to coverslips and imaged by fluorescence microscopy (Nikon, Tokyo, Japan) with a 60 × objective (NA. = 1.49). As control, 0.5% BSA was subjected to the same reaction and the product was imaged.

2.5. Transmission electron microscopy (TEM), atomic force microscopy (AFM), nanoparticle tracking analysis (NTA) and zeta potential measurement

The exosomes were diluted in PBS, fixed with 1% glutaraldehyde, applied onto a carbon-coated copper grid, and stained with 1% phosphotungstic acid. A JEM-2100 transmission electron microscope (JEOL, Tokyo, Japan) was employed to observe the specimens. AFM images were recorded using a BioScope Resolve system

and ScanAsyst imaging mode (Bruker, Billerica, MA, USA). Samples were prepared by applying a drop of exosomes at a concentration of 5 μg/mL onto mica; the samples were incubated until they were dry. Images were processed by NanoScope Analysis software (Bruker). NTA was performed using a NanoSight NS300 system (Malvern Instruments, Malvern, UK). The Brownian motion of exosomes suspended in PBS was recorded and tracked, generating size distribution data by applying the Stokes-Einstein equation. The zeta potentials of exosomes were measured using a Nano ZS90 device (Malvern) in 0.1 × PBS buffer at 25 °C.

2.6. Estimation of peptide quantity on the modified exosomes

c(RKDyK) with a fluorescein isothiocyanate (FITC) on the first lysine and an azide group on the last lysine was synthesized by NJPeptide Co. (Nanjing, China). The c[RK(FITC)DyK] was conjugated onto exosomes by the same reaction of cRGD-Exo fabrication. Then 1 mg/mL modified exosomes were solubilized by 0.5% Triton-100 to ensure FITC was not being quenched, and subjected to determine fluorescence. A standard curve of free c[RK(FITC)DyK] (0.1–0.9 μM) was used to calculated the molar concentration of c[RK(FITC)DyK] in exosome samples. According to the exosome particle concentration measured by NTA, the number of peptides on the exosome was estimated.

2.7. Flow cytometry

To examine the tropism of cRGD-Exo *in vitro*, 30 μg/mL Cy5.5-labeled exosomes (Cy5.5-Exo) or cRGD-Exo (Cy5.5-cRGD-Exo) or scrambled c(RDGyK) peptide-conjugated exosomes (Cy5.5-Scr-Exo) was incubated with integrin $\alpha_v\beta_3$-positive U87 cells or integrin $\alpha_v\beta_3$-negative HeLa cells at 37 °C for 3 h. For blocking experiments, cells were pre-incubated with c(RGDyK) peptide at 5, 20, 40 μM or scrambled c(RDGyK) peptide (Scr-pep) at 40 μM for 30 min prior to exosome adding. Subsequently, the cells were harvested by trypsinization, washed 3 times, and resuspended in PBS. In the mock group, untreated cells were collected and resuspended. The fluorescence intensity of over 20,000 cells from each sample was then measured with an Accuri C6 cytometer and analyzed with the CFlow software (BD Biosciences, San Jose, CA, USA). The percentage of Cy5.5-positive cells was determined *via* a comparison with the mock group, and the data were normalized to that of the Cy5.5-Exo group.

2.8. Co-culture of exosomes and cells

To investigate the uptake of cRGD-Exo by cells expressing and not expressing integrin $\alpha_v\beta_3$, U87-GFP cells and HeLa cells were co-cultured in the same dish and incubated with 50 μg/mL Cy5.5-Exo, Cy5.5-Scr-Exo, or Cy5.5-cRGD-Exo at 37 °C for 30 min. For blocking experiments, cells were pre-incubated with c(RGDyK) peptide or Scr-pep at 40 μM for 30 min prior to exosome adding. During the last 5 min of incubation, DiI, a lipophilic carbocyanine dye, was applied to stain the cell contours. Subsequently, the cells were washed and fixed with 4% paraformaldehyde, and 5 μg/mL Hoechst 33342 was used to stain the nuclei. A Ti-E microscope (Nikon) was then employed to observe the cells. Fluorescence at center wavelength/bandwidths of 440/44, 521/26, 607/34, and 700/45 was collected using a 40 × objective (NA. = 1.3) and recorded with an ORCA-ER cooled charge-coupled device (CCD) (Hamamatsu Photonics, Hamamatsu, Japan). The images were processed and analyzed using ImageJ software (NIH, Bethesda, MA, USA). Green staining indicated U87-GFP cells, and red cells that were not stained green corresponded to HeLa cells. The amounts of Cy5.5-Exo, Cy5.5-Scr-Exo, or Cy5.5-cRGD-Exo in the two types of cells were compared.

2.9. 2,3,5-Triphenyltetrazolium chloride (TTC) staining and lesion region demarcation

Twenty-four hours after reperfusion, the mouse brains were removed, coronally sliced at 1.5-mm intervals, and immersed in 0.25% TTC dye. After incubation at 37 °C for 30 min, photographs were taken. The pallor area indicated ischemic infarct, and the lesion region was demarcated according to previous reports with a minor modification [31,32]. Briefly, the initial 2-mm section (Section 1) from the anterior tip of the frontal lobe was removed by a coronal cut. The following 4-mm coronal section (Section 2) was obtained by another coronal cut. A longitudinal cut 1.5 mm from the midline through each hemisphere in Section 2 was then made to avoid the region supplied by the anterior cerebral artery. For the remaining two parts, the right was designated as the lesion region (ipsilateral), whereas the left corresponded to the non-ischemic region (contralateral).

2.10. Exosome administration

For the *in vivo* experiments, exosomes or curcumin was suspended in 0.2 mL PBS and administered *via* a single intravenous injection into the tail vein. Moreover, 0.2 mL PBS was intravenously administered as a control. To study targeting by NIRF imaging, 100 μg of Cy5.5-labeled exosomes, Scr-Exo, cRGD-Exo, or cRGD-Exo-cur was administered 12 h after reperfusion. The organs were then dissected 6 h after administration for analysis. To assess the therapeutic potential of cRGD-Exo-cur by quantitative PCR and Western blotting, 300 μg of unmodified exosomes, cRGD-Exo, or cRGD-Exo-cur or 50 μg curcumin was administered 12 h after reperfusion. The tissues corresponding to the lesion region were then dissected 12 h after administration for quantitative PCR or 24 h after administration for Western blotting.

2.11. NIRF imaging

Cy5.5-labeled exosomes were used for NIRF imaging. For the targeting study, 6 h after intravenous administration (18 h after reperfusion), the mice were anesthetized and sacrificed. The brain, heart, lungs, liver, spleen, and kidneys were dissected and fixed in 4% paraformaldehyde. An IVIS Spectrum imaging system (PerkinElmer, Waltham, MA, USA) was employed to capture NIRF images. The Cy5.5-related fluorescence signals were discriminated from the auto-fluorescence signals using Living Image software (PerkinElmer). For the time course experiments, 100 μg of Cy5.5-cRGD-Exo was administered 2, 6, 12, or 24 h after reperfusion. After 6 h of circulation, the brain was dissected, fixed and imaged.

2.12. Immunofluorescence staining and confocal imaging

For immunofluorescence assay, unmodified exosomes, Scr-Exo, or cRGD-Exo were labeled by the membrane intercalating dye PKH67 (Sigma), which gave brighter fluorescence under confocal scanning in comparison with Cy5.5. According to the previous report [33], 1.5 μL PKH67 was diluted in 100 μL diluent C, and 80 μL diluent C was added to the cRGD-Exo resuspended in 20 μL PBS. Subsequently, transfer the exosomes mixed with diluent C to the tube containing PKH67 in diluent C. After incubation for 3 min at RT, the reaction was stopped by adding 100 μL PBS containing 10% exosome-free FBS. Then, the exosomes were floated on a 30% sucrose/D_2O cushion and centrifuged at 164,000 g for 90 min using an SW41Ti rotor (Beckman Coulter) to remove unincorporated dye. After washing with PBS, the labeled exosomes were resuspended

and stored at −80 °C prior to use. To investigate the cellular localization of the exosomes in ischemic brain, 100 μg PKH67-labeled exosomes, Scr-Exo, or cRGD-Exo were intravenously administrated 12 h after reperfusion. Six hours later, the mice were perfused with 25 mL PBS and then with 25 mL 4% paraformaldehyde. The brains were isolated and cryosectioned in 40-μm thickness. The sections were treated by 0.3% Triton-100 for 30 min and by 3% BSA for 2 h, and then immunostained with anti-NeuN (Millipore), anti-GFAP (Millipore), anti-Iba-1 (Wako, Osaka, Japan), anti-Integrin α_v (Santa Cruz), or anti-CD34 (Abcam) antibodies over night at 4 °C. After washing 5 times by PBST (PBS containing 0.1% Triton-100), the samples were incubated with Alexa 594 or Alexa 647-conjugated secondary antibodies (Invitrogen, Grand Island, NY, USA) for 1 h at RT. After washing 5 times by PBST, staining by Hoechst 33342, and mounting with ProLong Antifade Reagents (Invitrogen), the tissue slides were imaged by an FV-1200 confocal microscope (Olympus, Tokyo, Japan). Images were processed and analyzed by ImageJ software (NIH). All settings of imaging and processing were kept constant, and the relative fluorescence intensities were calculated.

2.13. Curcumin incorporation and stability assays

To prepare cRGD-Exo-cur, 150 μg of curcumin (Sigma) was mixed with 900 μg of cRGD-Exo in PBS and allowed to incubate for 5 min at RT. Following a previous report [34], the mixture was subjected to sucrose gradient (8, 30, 45, or 60%) centrifugation for 90 min at 164,000 g using a SW41Ti rotor. A yellowish band between the 45 and 60% sucrose gradients was collected, washed, and resuspended in PBS. This fraction was designated cRGD-Exo-cur. To investigate the effect of exosomal incorporation on the stability of curcumin, curcumin and cRGD-Exo-cur were suspended in PBS at a concentration of 150 μg/mL and incubated in the dark at 37 °C. At different time points, the absorbance of each sample was measured at 450 nm using an Infinite F50 microplate reader (Tecan, Zürich, Switzerland). The experiments were repeated six times, and the absorbance was normalized to the initial values for each sample.

2.14. Quantitative real-time PCR

Twelve hours after intravenous administration (24 h after reperfusion), total RNA of the tissues corresponding to the lesion region was extracted by Trizol reagent (Invitrogen). The synthesis of cDNA was performed according to M-MLV reserve transcriptase instruction (Promega, Madison, WI, USA). PCR reactions were carried out by an ABI 7500 system in 20 μL reactions, with 1.5 μL cDNA samples, using SYBR Premix ExTaq (TaKaRa, Kusatsu, Japan). Relative expression was calculated by the comparative $2^{-\Delta\Delta Ct}$ method. All experiments were performed at least three times independently. The primers used were as follows: (forward) 5′-CCCCAGTCTGTATCCTTCTA-3′ and (reverse) 5′-CACTGTCCCAGCATCTTGT-3′ for TNFα; (forward) 5′-AAGGGCTGCTTCCAAAC-3′ and (reverse) 5′-TGTGCTGCTGCGAGATT-3′ for IL-1β; (forward) 5′-TACCACTCCCAACAGACC-3′ and (reverse) 5′-TTTCCACGATTTCCCAGA-3′ for IL-6; (forward) 5′-ATGTGGATCAGCAAGCAGGA-3′ and (reverse) 5′-AAGGGTGTAAAACGCAGCTCA-3′ for β-actin.

2.15. Western blot analysis

Twenty-four hours after intravenous administration (36 h after reperfusion), the tissues corresponding to the lesion region were dissected from the mice, and homogenized in RIPA buffer with Protease Inhibitor Tablets (Pierce). After centrifugation at 12,000 rpm for 30 min at 4 °C, the supernatants were collected for SDS-polyacrylamide gel electrophoresis (Bio-Rad, Hercules, CA, USA). The samples were subsequently transferred to polyvinylidene difluoride membrane (Millipore) and incubated with the primary antibodies as follows: anti-TNFα was from Abcam, anti-IL-1β, anti-IL-6, anti-p-p65, and anti-cleaved caspase-3 were from Cell Signaling Technology (Danvers, MA, USA). After incubation with horseradish peroxidase-conjugated secondary antibodies, the signals were visualized by a chemiluminescence system (Bio-Rad). ImageJ software was employed to perform densitometric analysis.

2.16. Statistical analysis

The data are presented as mean ± SEM. Statistical analysis was accomplished using GraphPad Prim software (GraphPad Software, San Diego, CA, USA). Comparison between two groups was performed by Student's *t*-test. The significances among multiple groups were determined by One-way Analysis of Variance (ANOVA) followed by Bonferroni *post hoc* test. P value < 0.05 was considered statistically significant.

3. Results

3.1. Preparation and characterization of cRGD-Exo

Mouse bone marrow-derived MSCs were cultured and exosomes were isolated from their conditioned medium by ultracentrifugation. TEM was used to reveal vesicles with diameters of 40–150 nm (Fig. 1A and B). Western blot analysis showed that Alix and TSG101 (known exosomal markers) were enriched in the exosome pellet fraction, whereas Calnexin, expressed in endoplasmic reticulum, was not detected in exosomes (Fig. 1C).

To conjugate exosomes with c(RGDyK), a two-step reaction was proposed (Fig. 1D). First, DBCO groups were introduced to the exosome surface by cross-linking exosomes with DBCO-sulfo-NHS. The NHS groups were incorporated with the amino groups on the exosomal proteins or phosphatidylethanolamine to form covalent bonds. Second, the DBCO groups on the exosomes reacted with azide-functionalized c(RGDyK) to form stable triazole linkages using copper-free click chemistry. To track the exosomes, Cy5.5 azide was also conjugated to the DBCO groups. This method is easy, fast and flexible. All the reactions were performed in physiological, neutral aqueous buffer without any catalyst.

The morphology of unmodified exosomes and cRGD-Exo were assessed by TEM (Fig. 1A and B) and AFM (Fig. 1E and F). Specifically, unmodified exosomes were round in shape, with an average diameter of 92 nm. Upon conjugation of c(RGDyK), the mean diameter of exosomes increased to 131 nm. According to the AFM images, the cRGD-Exo was round in shape and well dispersed. Next, the size distributions of unmodified and modified exosomes were evaluated using NTA, which showed that the highest peak of both profiles were around 100 nm (Fig. 1G). Although the profile of cRGD-Exo yielded peaks exceeding 150 nm, 75% of the cRGD-Exo was <150 nm in size and 92% was <200 nm in size. Furthermore, the zeta potential of the unmodified exosomes was measured to be −26.4 mV, which is consistent with previous findings [35]. The zeta potential of the cRGD-Exo increased to −21.6 mV. As a control, a scrambled c(RDGyK) peptide was conjugated onto exosomes (Scr-Exo) which showed a zeta potential of −20.7 mV, similar to that of cRGD-Exo. The size distributions of Scr-Exo were also similar to that of cRGD-Exo (Supplementary Fig. S1). To estimate the number of peptide on the modified exosomes, a fluorescent cyclic peptide c[RK(FITC)DyK] was conjugated and the fluorescence of the resultant exosomes was assessed. By comparison to a fluorescent standard curve of free c[RK(FITC)DyK], it was calculated that 1 mg/mL modified exosomes contained an average of 523 nM peptides (Supplementary Fig. S2). By calculating the exosome number using

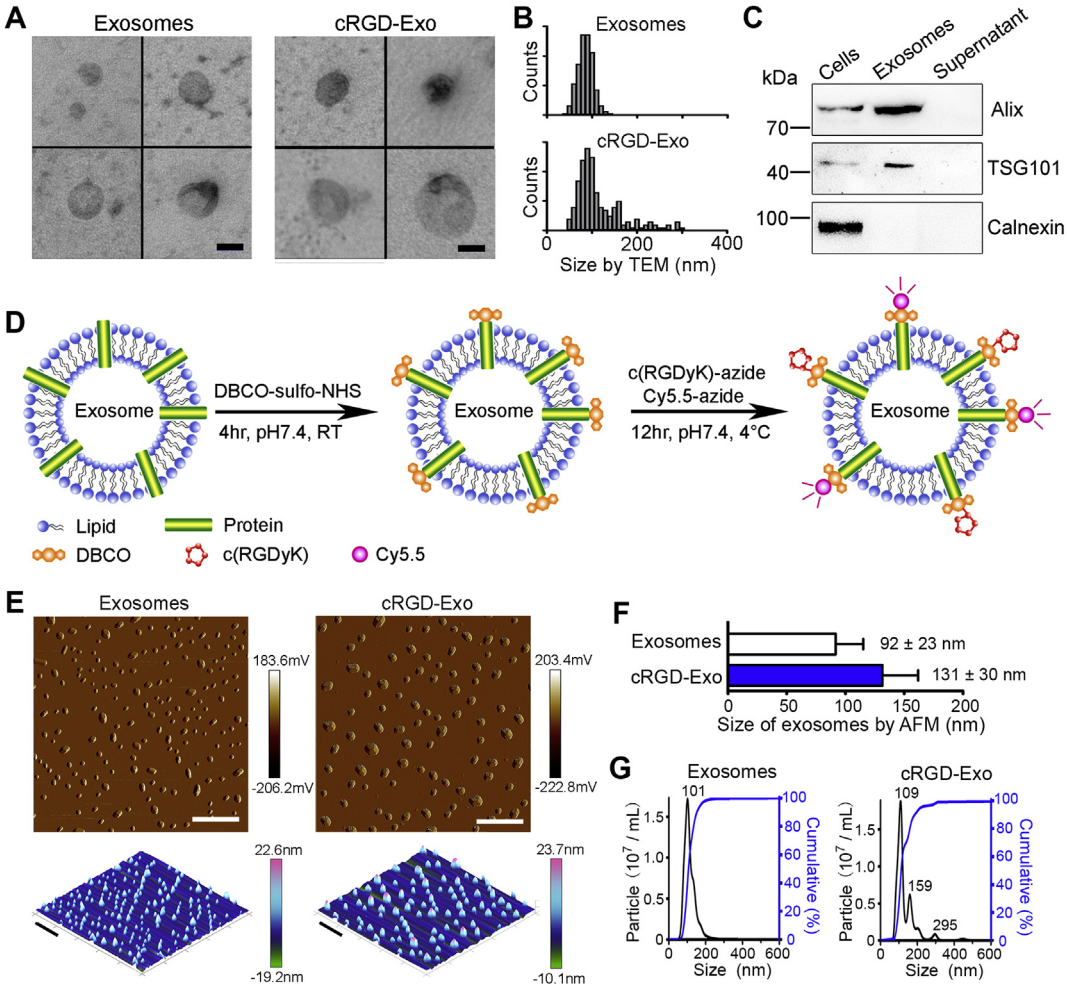

Fig. 1. Modification and characterization of exosomes. (A) Transmission electron micrograph of unmodified exosomes and the cRGD-Exo. Scale bar, 100 nm. (B) Size distribution of unmodified exosomes and the cRGD-Exo measured from TEM images. (C) Western blot analysis of Alix, TSG101, and Calnexin from MSCs and exosomes isolated from their conditioned medium. The supernatant obtained from the ultracentrifugation during exosome isolation was used as a negative control. (D) Schematic diagram of conjugating c(RGDyK) and Cy5.5 fluorophor to exosomal amine groups by a two-step reaction. (E) AFM images of unmodified exosomes and the cRGD-Exo. Upper graphs show peak force error images. Lower graphs present 3D height sensor images. Scale bar, 1 μm. (F) Statistics of the size of exosomes based on ten AFM images. Data are shown as mean ± SD. (G) Size distributions of unmodified exosomes and the cRGD-Exo based on NTA measurements.

NTA, It was estimated that approximately 263 peptides were conjugated onto one exosome.

3.2. Cellular tropism of cRGD-Exo in vitro

Fluorescence microscopy revealed small particles corresponding to Cy5.5-conjugated exosomes or Scr-Exo or cRGD-Exo (Fig. 2A, and Supplementary Fig. S3A). As a control, 0.5% bovine serum albumin (BSA) was subjected to the same conjugation treatment as the exosomes but the product showed no fluorescence. The morphology and the size distributions of Cy5.5-conjugated exosomes were assessed by TEM and NTA (Supplementary Fig. S3B and C). To investigate the tropism of cRGD-Exo, exosome uptake was assessed on HeLa and U87 cells which express different integrin patterns. Consistent with previous reports [36–38], Western blot analysis showed that HeLa cells express $\alpha_5\beta_1$, $\alpha_v\beta_5$, some $\alpha_{IIb}\beta_3$, but almost no expression of $\alpha_v\beta_3$, whereas U87 cells express high levels of $\alpha_v\beta_3$ (Fig. 2B). Flow cytometry based on the fluorescence intensity of exosomes was then employed to analyze the level of internalization. Specifically, the uptake efficiencies of exosomes and cRGD-Exo and Scr-Exo by $\alpha_v\beta_3$-negative HeLa cells showed no significant difference. Conversely, the uptake level of cRGD-Exo by $\alpha_v\beta_3$-positive U87 cells was 3-times higher than that of exosomes or Scr-Exo, which was inhibited by using c(RGDyK) peptide dose-dependently (Fig. 2C and D). Moreover, U87-GFP and HeLa cells were co-cultured and incubated with Cy5.5-labeled exosomes (Supplementary Fig. S3D). Fluorescence microscopy showed that cRGD-Exo (magenta), but not exosomes or Scr-Exo, entered more efficiently into U87 cells (green) as compared to HeLa cells (Fig. 2E, and Supplementary Fig. S3E). These results indicate that this biochemical method effectively conjugates the c(RGDyK) peptide onto the surface of exosomes and that the resulting cRGD-Exo exhibits a high affinity/specificity to cells expressing integrin $\alpha_v\beta_3$.

3.3. The ability of cRGD-Exo to target to the ischemic brain

To evaluate cRGD-Exo in targeting ischemic brain *in vivo*, mice were subjected to MCAO/R in the right hemisphere, and infarct areas were confirmed based on TTC-stained brain sections (Fig. 3A). In general, the lesion region consists of an irreversibly damaged ischemic core and a surrounding salvageable region known as the penumbra [39]. In this well-established animal model, the ischemic core appears in the lateral striatum and spreads to the overlying cortex, while the penumbra is primarily located in the adjacent

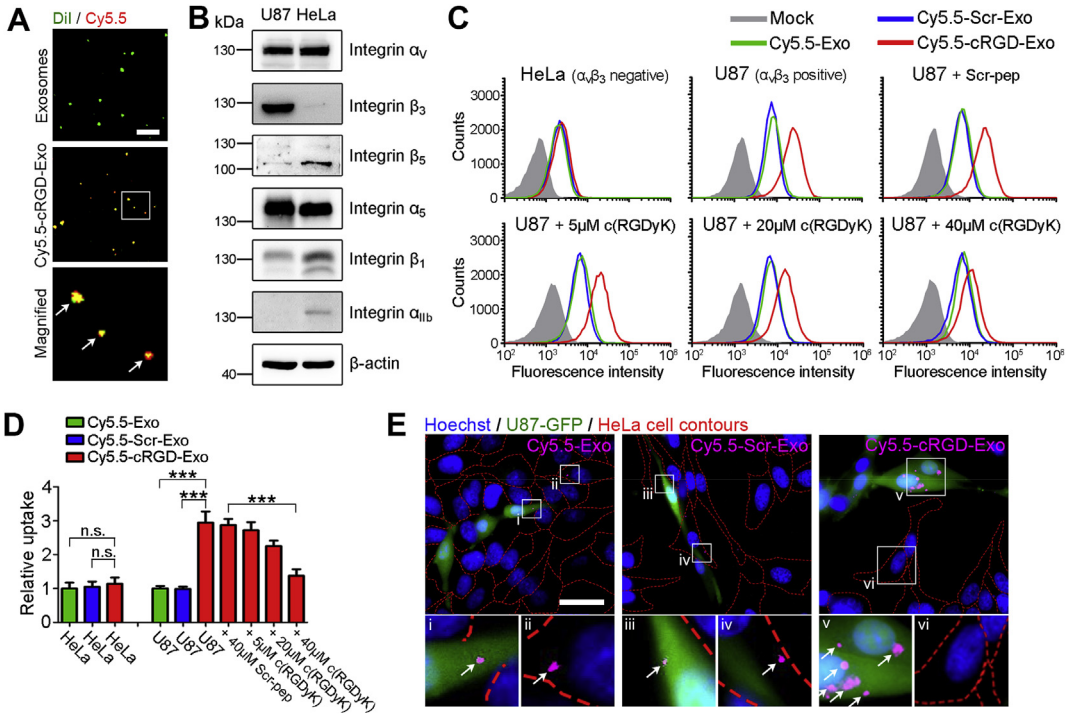

Fig. 2. The cellular tropism of cRGD-Exo *in vitro*. (A) Fluorescence image of unmodified or modified exosomes. Green shows DiI-stained lipid membranes. Red is Cy5.5. Arrows indicate the co-localization between DiI and Cy5.5 on exosomes. Scale bar, 5 μm. (B) Western blot analysis of integrin subunits α_v, β_3, β_5, α_5, β_1, α_{IIb} from U87 and HeLa cells. (C) Flow cytometric analyses of Cy5.5-labeled exosomes (green, as control) or Scr-Exo (blue) or cRGD-Exo (red) uptake by U87 cells or HeLa cells. (D) The relative percentage of Cy5.5-positive HeLa or U87 cells determined in comparison with the mock group and normalizing to the Cy5.5-Exo group. Data are expressed as mean ± SEM. n = 5; n.s., not significant; $^*P < 0.05$, $^{***}P < 0.001$ by student's *t*-test. (E) Representative fluorescence images of cellular uptake of Cy5.5-labeled exosomes or Scr-Exo or cRGD-Exo after 30-min incubation with U87-GFP and HeLa cells. Green shows U87-GFP cells. HeLa cell contours were distinguished by DiI (red dashed lines). Blue indicates nuclei. Magenta represents Cy5.5-labeled exosomes, Scr-Exo, or cRGD-Exo. Lower panel shows enlarged graphs with arrows indicating internalized exosomes in cells. Scale bar, 30 μm.

ventrolateral neocortex [32]. Following previous reports [31,32], the typical lesion region (ipsilateral) and matching non-ischemic region (contralateral) are shown in Fig. 3B.

To examine the ability of cRGD-Exo to target the ischemic brain, Cy5.5-labeled exosomes, Scr-Exo, or cRGD-Exo was intravenously injected in mice which received 1 h of MCAO and 12 h of reperfusion. Six hours later, brains were dissected and analyzed by NIRF imaging (Fig. 3C). The fluorescence intensity of the lesion region was significantly higher after cRGD-Exo administration as compared to unmodified exosomes (Fig. 3D). Notably, the fluorescence ratio of the ipsilateral to the contralateral region increased dramatically to as high as 11 following cRGD-Exo injection (Fig. 3E). These results indicate that c(RGDyK) conjugation significantly enhances the tropism to the lesion region of the ischemic brain. The enhanced tropism of cRGD-Exo to the ischemic brain should be attributable to integrin $\alpha_v\beta_3$. This molecule is related to the angiogenic response to brain ischemia, is expressed on reactive endothelial cells after ischemia, and exhibits sustained increases in expression [26,27]. Vessels in both the ischemic core and penumbra showed a strong increase in integrin $\alpha_v\beta_3$ expression, whereas the non-ischemic region expressed little integrin $\alpha_v\beta_3$ [40].

Next, different organs of mice were dissected and quantitatively analyzed by NIRF imaging to study exosome biodistribution (Fig. 3F and G). To get a better contrast of the image, each organ was imaged separately (Supplementary Fig. S4). Unmodified exosomes primarily accumulated in the liver, followed by the kidneys, and then the brain and lungs. Interesting, cRGD-Exo injection increased the signal in the brain, liver, and lungs compared with those following unmodified exosome treatment. The increase in brain targeting of cRGD-Exo compared to unmodified exosomes was greater than the corresponding increase in the liver and lungs. These results are consistent with those of previous studies on cRGD-modified nanoparticles [41,42]. From literature, the increase accumulation of cRGD-Exo in the liver is resulted from high levels of integrin $\alpha_v\beta_3$ in liver [43], while the slight more entrapment in the lungs due to the larger size of cRGD-Exo [44]. The biodistribution of free Cy5.5 azide, a control, exhibited a significantly different pattern (Supplementary Fig. S5).

Furthermore, to evaluate the kinetics of the modified exosome brain tropism, cRGD-Exo was intravenously injected 2, 6, 12, and 24 h after MCAO/R as well as 12 h after sham ischemia. Brains were collected 6 h after each injection to assess brain tropism *via* NIRF imaging. As shown in Fig. 3H–J, the targeting behavior of cRGD-Exo was evident 12 h after reperfusion, and its efficiency increased at 24 h. These results are most likely correlating with the level of integrin $\alpha_v\beta_3$ expression [26,27]. Actually, 12–24 h after stroke is an effective time window for therapy, such as suppression of inflammation [45].

3.4. Cellular localization of cRGD-Exo in ischemic cerebral tissue

To perform further histological investigation, brains were sectioned after 1 h of MCAO and 12 h of reperfusion. Integrin α_v and β_3 were labeled by immunofluorescence and examined under a confocal microscope. Strong co-localization between integrin α_v/β_3 and CD34, a marker of endothelial cells, was found in the lesion region (ipsilateral) (Fig. 4A, and Supplementary Fig. S6A). In contrast, integrin α_v/β_3 and CD34 overlap was minimal in the non-ischemic region (contralateral). These results are in line with previous reports on integrin $\alpha_v\beta_3$ expression in reactive vascular endothelial cells, induced by ischemia [26,27]. In addition, integrin β_3 was also detected in microglia to a lesser extent by co-labeling

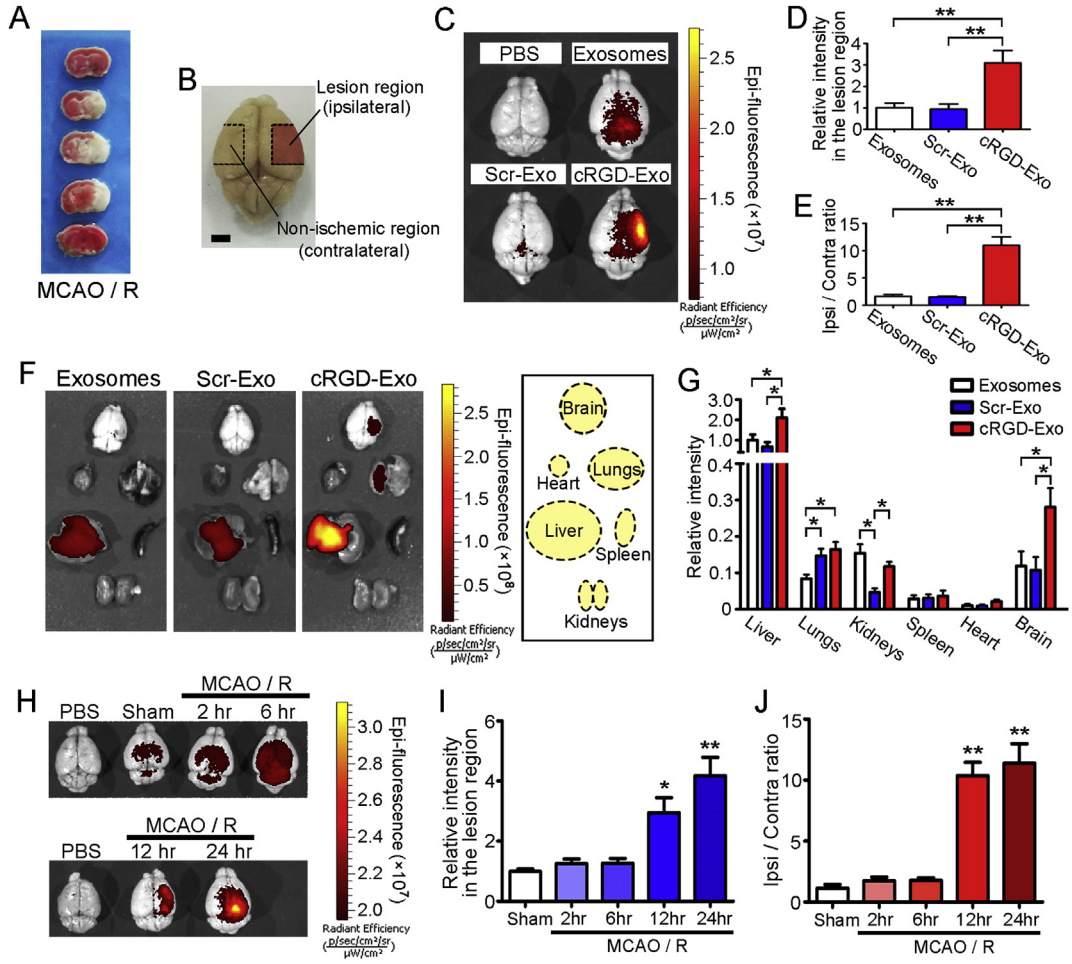

Fig. 3. Ability of cRGD-Exo to target the lesion region of ischemic brain. (A) TTC-stained brain sections show the typical infarct area in a mouse receiving 1 h of MCAO and 24 h of reperfusion. (B) Illustration of the lesion region (including ischemic core and penumbra; ipsilateral, around by dashed lines and overlaid with reddish) of ischemic brain. Matching non-ischemic region is also indicated (contralateral, around by dashed lines without overlay). Scale bar, 2 mm. (C) Representative NIRF images (overlaid with photograph) of mice brains which received MCAO/R and the administration of PBS, Cy5.5-labeled exosomes, Scr-Exo or cRGD-Exo. Brains were dissected 6 h after administration (18 h after reperfusion). (D) Quantitation of fluorescence intensity in the lesion region. (E) Normalized ratios of fluorescence intensity in ipsilateral versus contralateral region. Data in D and E are expressed as mean ± SEM. n = 5; $^{**}P < 0.01$ by One-way ANOVA. (F) Representative NIRF images of organs dissected from mice which received MCAO/R along with the administration of Cy5.5-labeled exosomes, Scr-Exo, or cRGD-Exo. Organs were dissected 6 h after administration (18 h after reperfusion). Right boxed graph illustrates location of the analyzed six organs. (G) Quantitation of fluorescence intensities in different organs. Data are expressed as mean ± SEM. n = 4; $^{*}P < 0.05$ by student's *t*-test. (H) Representative NIRF images of mice brains which received MCAO/R and cRGD-Exo at different time points post-reperfusion. Brains were dissected 6 h after administration. The brain from sham mice that received cRGD-Exo administration was also imaged. Quantitative curves showing (I) the fluorescence intensities in the lesion region and (J) the ipsilateral/contralateral ratios following cRGD-Exo administration at different time points. Data are expressed as mean ± SEM; n = 4; $^{*}P < 0.05$, $^{**}P < 0.01$ by One-way ANOVA.

with ionized calcium-binding adapter molecule 1 (Iba1) (Supplementary Fig. S6B). In fact, it is well documented that integrin $\alpha_v\beta_3$ is expressed by microglia and regulated by cytokines [46].

Next, PKH67-labeled exosomes, Scr-Exo, or cRGD-Exo was intravenously administered to mice receiving 1 h of MCAO and 12 h of reperfusion to assess the ability of cRGD-Exo to bind integrin $\alpha_v\beta_3$ on vascular endothelial cells. After 1 h of blood circulation, brain tissues were sectioned and analyzed by confocal microscopy. cRGD-Exo co-localized with integrin α_v/β_3 and CD34 strongly in the lesion region (Fig. 4B and C, and Supplementary Fig. S7A). In contrast, exosomes/Scr-Exo and integrin α_v/β_3 or CD34 overlap was minimal (Supplementary Fig. S7B and Fig. S8). Interestingly, after 6 h of blood circulation, the co-localization between cRGD-Exo and endothelial cells decreased dramatically. cRGD-Exo appeared in brain cells near the blood vessels (Fig. 4C). Also, high fluorescence signal was observed in the ipsilateral striatum and overlying the cortex, the main vulnerable areas during MCAO/R (Supplementary Fig. S9). In contrast, fluorescence signals in matching contralateral areas were much lower. Magnified images clearly show that the fluorescence was entrapped in vesicular compartments near the cell nuclei. These results indicate that cRGD-Exo bind integrin $\alpha_v\beta_3$ on endothelial cells, migrate to brain tissue, and enter brain cells in the lesion region.

Furthermore, the specific cell types targeted by cRGD-Exo were investigated by staining brain sections for Iba1, neuronal nuclear antigen (NeuN), and glial fibrillary acid protein (GFAP), markers for microglia, neurons, and astrocytes, respectively. Interestingly, the cRGD-Exo signal was detected in not only integrin $\alpha_v\beta_3$-positive microglia, but also neurons and astrocytes, which lack integrin $\alpha_v\beta_3$ expression (Fig. 4D). This result may be attributable to surface proteins on exosomes that may be involved in cell binding and uptake. For instance, the neuronal uptake of MSC-derived exosomes can be mediated by the interaction of vesicle-associated membrane protein 2 (VAMP2) on exosomes and synaptosomal-associated protein 25 (SNAP-25) at the plasma membrane [47].

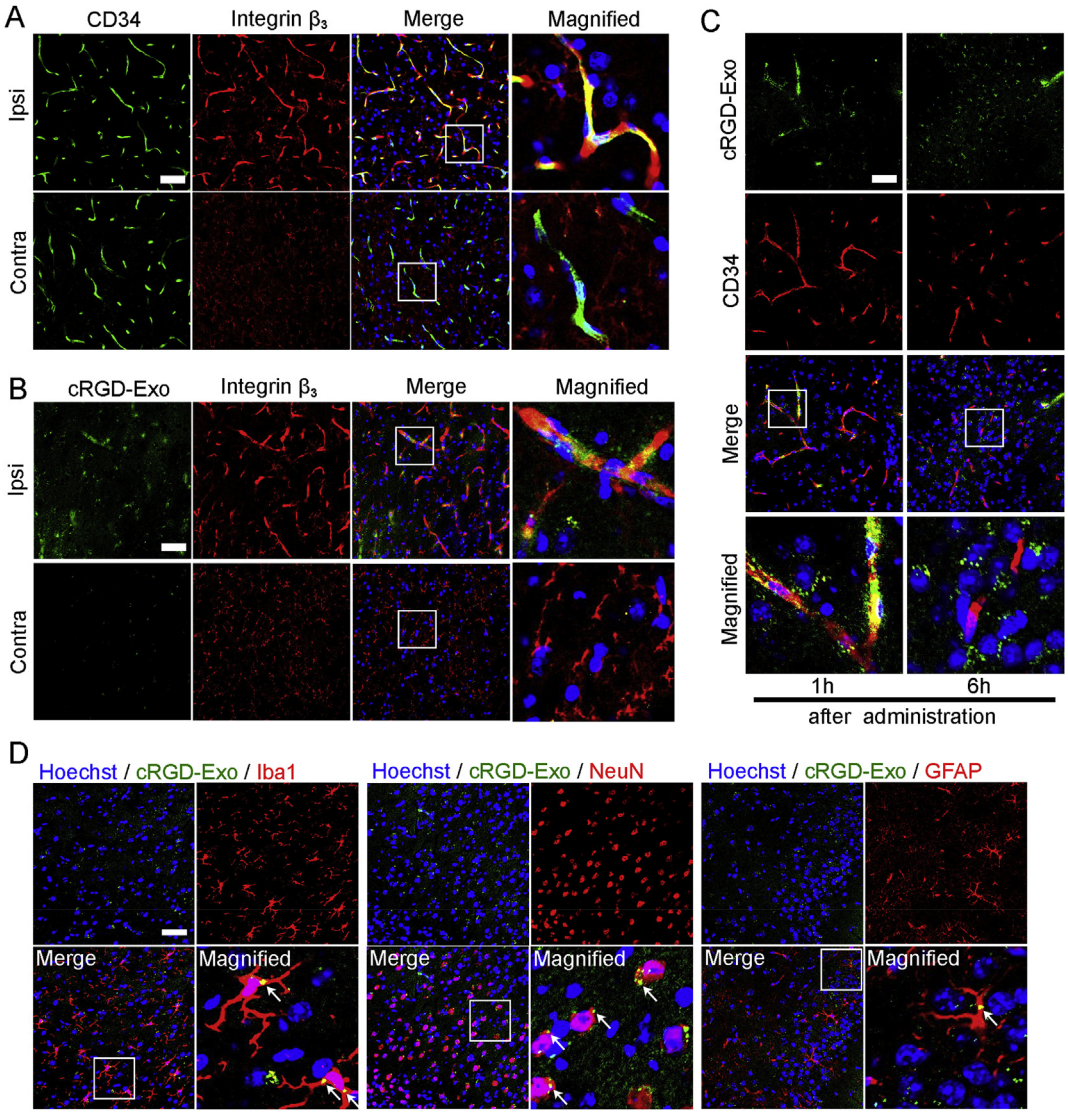

Fig. 4. Evaluation of the cellular localization of cRGD-Exo in ischemic cerebral tissue. (A) Co-labeled fluorescence images of vascular endothelial cells (CD34, green) with integrin β_3 (red) in the lesion region (ipsilateral) and non-ischemic region (contralateral) 12 h after reperfusion. (B) Co-labeled fluorescence images of cRGD-Exo (green) with integrin β_3 (red) in the lesion region and non-ischemic region 1 h after intravenous administration (13 h after reperfusion) of PKH67-labeled cRGD-Exo. (C) Co-labeled fluorescence images of cRGD-Exo (green) with CD34 (red) in the lesion region 1 h or 6 h after intravenous administration (13 h or 18 h after reperfusion) of cRGD-Exo. (D) Co-labeled fluorescence images of cRGD-Exo (green) with microglia (Iba1), neuron (NeuN), or astrocytes (GFAP) in the lesion region 6 h after intravenous administration (18 h after reperfusion) of cRGD-Exo. Arrows indicate internalized cRGD-Exo in cells. Blue indicates nuclei. Scale bar, 50 μm.

3.5. Characterization of curcumin-containing cRGD-Exo and their targeting capability

The suppression of inflammation holds great promise among the potential therapeutic approaches for ischemic stroke. Because these treatments extend therapeutic window up to 12–24 h post-ischemia and the inflammatory response plays an important role in brain injury produced by ischemia, particularly during reperfusion [45]. Curcumin is a promising natural drug for the treatment of ischemic stroke due to its powerful anti-inflammatory activity [48]. However, despite extensive research and development, the poor solubility, instability, and low bioavailability of curcumin limits its clinical efficacy. Based on the curcumin binding capacity of exosomes reported by Sun et al. [34], the cRGD-Exo was loaded with curcumin (cRGD-Exo-cur) by mixing cRGD-Exo and curcumin at a 6:1 ratio (protein weight/weight), followed by sucrose gradient centrifugation. The degradation curves of free curcumin and cRGD-Exo-cur showed that exosomal entrapment protected curcumin from degradation (Fig. 5A). In addition, cRGD-Exo-cur remained round in shape, as analyzed by AFM and TEM (Fig. 5B–E). Compared with cRGD-Exo, the mean size of cRGD-Exo-cur increased to 145 nm and exhibited a larger standard deviation (Fig. 5D). Specifically, 62% of cRGD-Exo-cur were <150 nm and 73% were <200 nm according to NTA data (Fig. 5F). Moreover, the zeta potential of the cRGD-Exo-cur was measured to be −26.1 mV, similar to that of the unmodified exosomes. As control, unmodified exosomes and Scr-Exo were also loaded with curcumin (Exo-cur and Scr-Exo-cur) and then characterized by TEM and NTA (Fig. 5E and F, and Supplementary Fig. S10).

To examine the effect of curcumin incorporation on targeting capability of cRGD-Exo, Cy5.5-labeled cRGD-Exo-cur were administered in mice subjected to MCAO/R and was allowed to circulate for 6 h. Surprisingly, fluorescence in the lesion region was

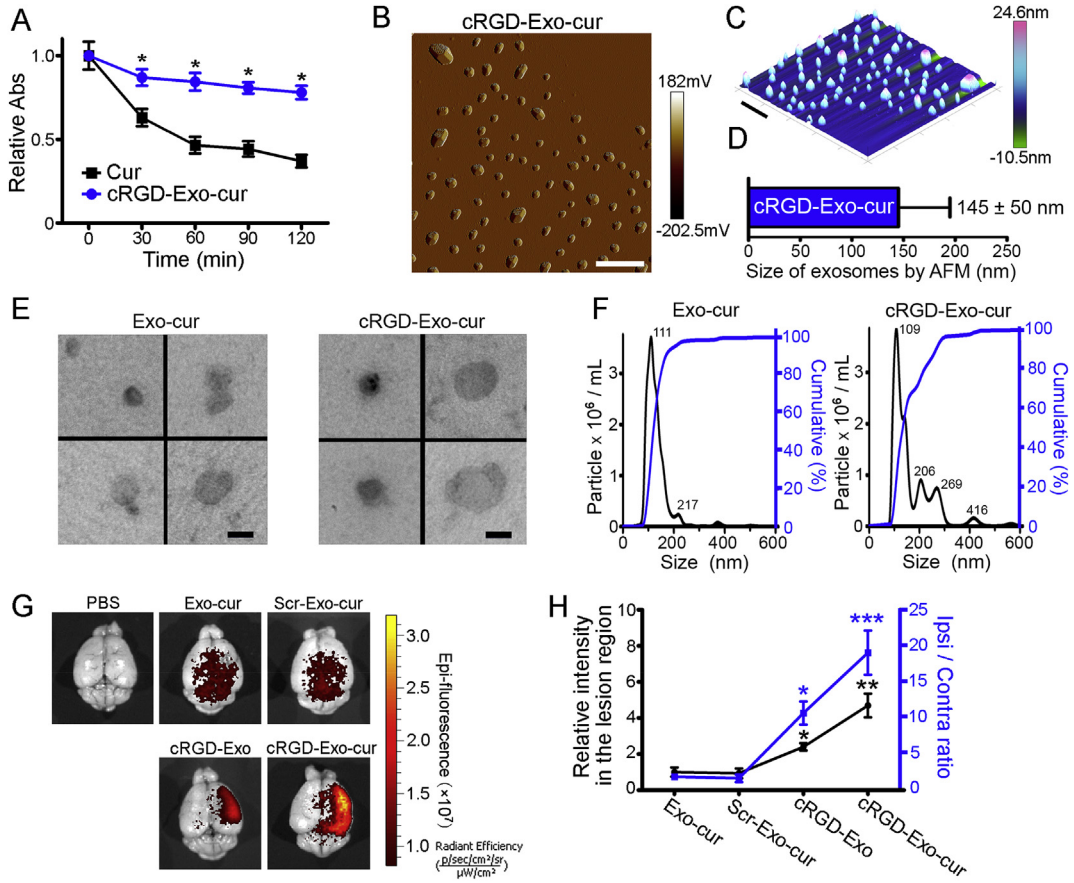

Fig. 5. Characterization of cRGD-Exo-cur and their capability of targeting the lesion region of ischemic brain. (A) Curcumin and cRGD-Exo-cur were suspended in PBS and incubated in the dark at 37 °C. Curves of the absorbance at 450 nm show their concentration changes within 120 min. Data are expressed as mean ± SEM. n = 6; $^{*}P < 0.05$ versus the curcumin group at the same time point by student's *t*-test. (B) Peak force error image and (C) 3D height sensor image of the cRGD-Exo-cur obtained by AFM. Scale bar, 1 μm. (D) Statistics of the exosome sizes measured from 10 AFM images. Data are shown as mean ± SD. (E) Transmission electron micrograph of Exo-cur and cRGD-Exo-cur. Scale bar, 100 nm. (F) Size distributions of Exo-cur and cRGD-Exo-cur based on NTA measurements. (G) Representative NIRF images (overlaid with photograph) of mice brains which received MCAO/R and administration of PBS, Cy5.5-labeled Exo-cur, Scr-Exo-cur, cRGD-Exo or cRGD-Exo-cur. (H) Quantitative analysis shows the relative fluorescence intensities in the lesion region (black dots) and the ipsilateral/contralateral ratios (blue squares) following administration of Exo-cur, Scr-Exo-cur, cRGD-Exo or cRGD-Exo-cur. Data are expressed as mean ± SEM. n = 4; $^{*}P < 0.05$, $^{***}P < 0.001$ by One-way ANOVA.

significant stronger after injection of cRGD-Exo-cur, as compared to cRGD-Exo or Exo-cur or Scr-Exo-cur, with the ipsilateral/contralateral ratio as high as 19, indicating that curcumin incorporation improved the delivery efficiency (Fig. 5G and H). Furthermore, the biodistribution of exosomes showed that cRGD-Exo-cur administration generally enhanced the fluorescence intensities in most organs compared with those following cRGD-Exo treatment, suggesting that the enhancement induced by curcumin incorporation is non-specific (Supplementary Fig. S11). These results are consistent with previous reports showing that curcumin loading enhances the uptake of polymer micelles into cells [49]. Specifically, curcumin can be self-assembled into the lipid bilayer of exosomes through the hydrophobic interaction [34]. Thus, the incorporation of curcumin can increase the number of hydrophobic moieties in exosome membrane, leading to enhanced internalization of curcumin-loaded exosomes [49].

3.6. The inhibition of cRGD-Exo-cur on the post-ischemia inflammatory response

After ischemic stroke, several pro-inflammatory cytokines, such as tumor necrosis factor-α (TNF-α), interleukin-1β (IL-1β), and interleukin-6 (IL-6), mediate the inflammatory response [50]. In fact, TNF-α, IL-1β, and IL-6, whose expression levels increase in the early phase after human and experimental stroke and remain elevated for days, are responsible for infarct evolution and tissue injury [51]. In the mouse MCAO/R model, the TNF-α, IL-1β, and IL-6 mRNA expression levels increase within 4–6 h of reperfusion and peak at 18–24 h [51]. To confirm the therapeutic potential of curcumin-loaded targeting exosomes, cRGD-Exo-cur were injected *via* the tail vein 12 h after MCAO/R. mRNA and protein expression levels of the three pro-inflammatory cytokines in the lesion region of the ischemic brain were then evaluated 12 h later (24 h of reperfusion) and 24 h later (36 h of reperfusion). As shown in Fig. 6A–C, mice treated with cRGD-Exo-cur expressed significantly lower levels of TNF-α, IL-1β, and IL-6 compared to mice treated with curcumin alone. Next, the activation of microglia, which is associated with neuro-inflammation, was assessed. Twenty-four hours after administration (36 h of reperfusion), tissues were stained for Iba1, a marker of microglia activation. Because microglias in the ischemic core are degenerated and fragmented, microglias were observed in the peri-infarct area (Fig. 6D). In the sham group, microglia with ramified thin processes and small cellular bodies were observed in their resting form. In contrast, MCAO/R induced strongly stained microglia with highly branched processes. Upon cRGD-Exo-cur administration, the fluorescence intensity of activated microglia was significantly lower than curcumin treatment alone (Fig. 6E). Previous reports have

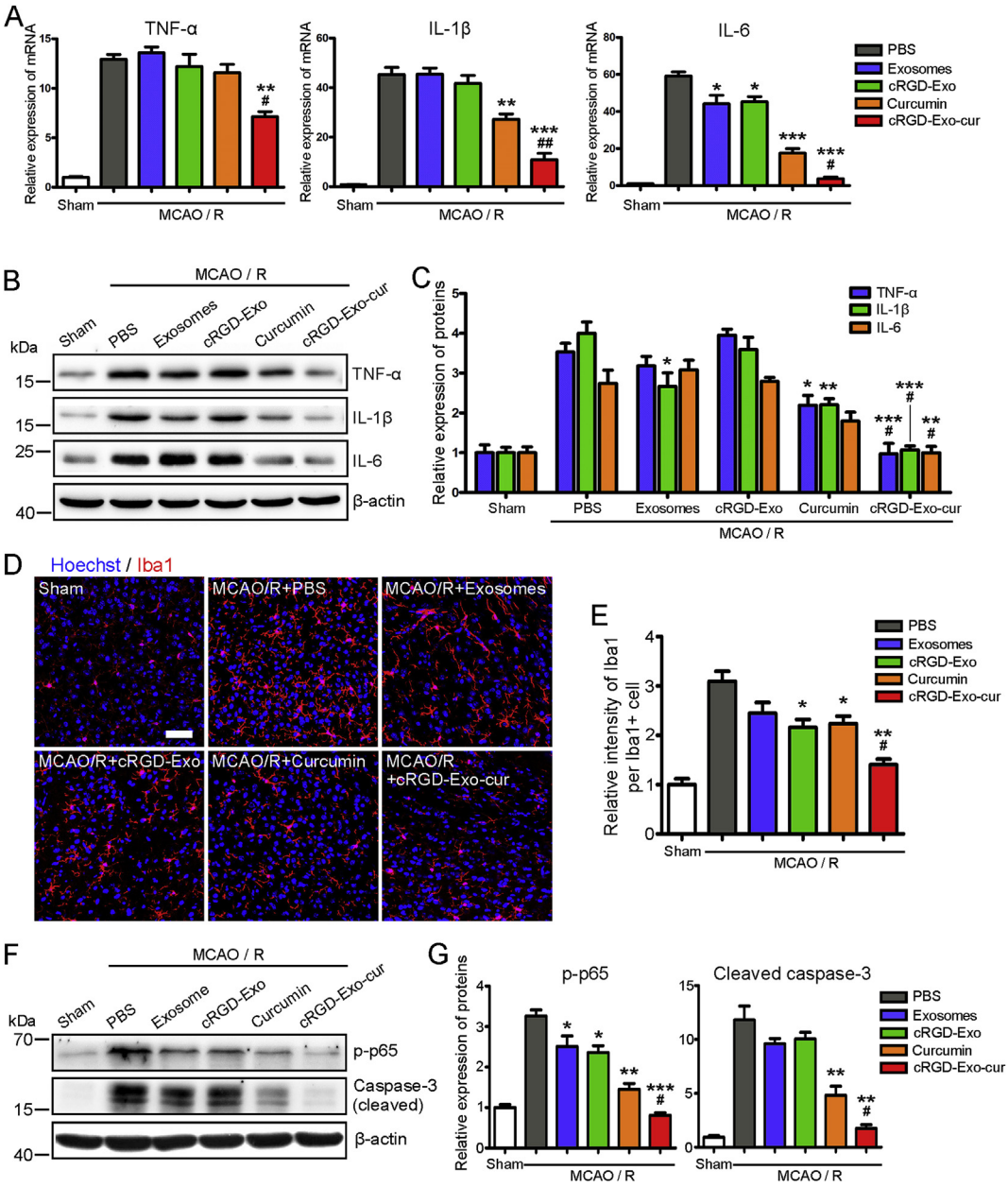

Fig. 6. The inhibitory effect of cRGD-Exo-cur on inflammatory response after cerebral ischemia. Intravenous administrations of PBS, unmodified exosomes, cRGD-Exo, curcumin, or cRGD-Exo-cur were performed on mice receiving 1 h of MCAO and 12 h of reperfusion. (A) RT-PCR analyses of TNF-α, IL-1β, and IL-6 in the tissue of lesion region were performed 12 h after administration (24 h after reperfusion). (B) Western blot and (C) quantitative analyses of TNF-α, IL-1β, and IL-6 in the tissue of lesion region were performed 24 h after administration (36 h after reperfusion). (D) Representative fluorescence images of Iba1 stained microglia at peri-infarct areas 24 h after administration (36 h after reperfusion). Scale bar, 50 μm. (E) Quantitative analysis showing the fluorescence intensity of Iba1 per cell corresponding to (D). (F) Western blot and (G) quantitative analyses of p-p65 and cleaved caspase-3 in the tissue of lesion region were performed 24 h after administration (36 h after reperfusion). The sham groups were used as negative control. Data are expressed as mean ± SEM. n ≥ 4; $^{*}P < 0.05$, $^{**}P < 0.01$, $^{***}P < 0.001$ versus the PBS groups, and $^{\#}P < 0.05$, $^{\#\#}P < 0.01$ versus the Curcumin groups by One-way ANOVA.

demonstrated that MSC-derived exosomes harness intrinsic immunosuppressive activity [52,53]. Consistently, unmodified exosomes and cRGD-Exo also showed an anti-inflammatory effect, but this effect seems to be less significant than that of curcumin.

Furthermore, the anti-inflammatory activity of curcumin is known to be mediated by modulation of several crucial transcription factors, including nuclear factor κB (NF-κB) [54]. Thus, we evaluated the level of phosphorylated p65 (p-p65), the active form of NF-κB subunit, 24 h post-injection and observed that cRGD-Exo-cur more effectively inhibited p-p65 expression in the lesion region as compared to unmodified exosomes, cRGD-Exo, or free curcumin (Fig. 6F and G). Next, the expression of cleaved caspase-3, the active form of an apoptotic protease, was detected by Western blotting which was suppressed in cRGD-Exo-cur treated mice. In addition, the therapeutic efficacy of cRGD-Exo-cur was dose-dependent by comparison with free cur (Supplementary Fig. S12). Finally, no obvious liver toxicity or tissue damage was observed in the cRGD-Exo or cRGD-Exo-cur treated mice compared with the control group (Supplementary Fig. S13). Overall, these results indicate that cRGD-Exo-cur better suppressed the inflammatory response after cerebral ischemia as compared to free curcumin, and did not cause apparent toxicity or tissue damage.

4. Discussion

Ischemic stroke remains a major cause of death and disability that lacks effective treatment after 4.5 h [1,3]. Anti-inflammation holds great promise to extend therapeutic window and prevent major brain injury during reperfusion. Exosomes are believed to be a potential therapeutic tool, given their unique properties, including low immunogenicity, biodegradability, low toxicity, strong protection for cargo and the ability to cross the BBB [15,16,19]. However, the intravenous delivery of exosomes into the ischemic brain remains a challenge due to poor targeting of unmodified exosomes [17,18]. Many previous studies highlighted the engineering of exosomes for the enhancement of therapeutic capability [16,19,20]. But an easy, rapid and efficient method for exosomes modification with targeting moiety is still lacking. Herein, we proposed a universal strategy to easily and rapidly modify the exosome surface by bio-orthogonal chemistry. Using this method, a c(RGDyK) peptide and a fluorophore were conjugated onto exosomes isolated from the conditioned medium of MSCs. Compared with existing "cell engineering" approaches, this robust and scalable method can be applied to any exosomes preisolated from culture medium or body fluids, and various moieties can be conjugated to the exosome surface within 24 h. In addition, multiple ligands with disparate characteristics can be simultaneously conjugated, and the ligand densities can be fine-tuned by adjusting the ratio of reactants. Furthermore, the copper-free click chemistry used here is very biocompatible and bio-orthogonal, and has been applied in living cells, zebrafish, and mice without apparent toxicity or physiological perturbation [55–57]. Hence, it is hypothesized that the integrity of the exosomes and the bioactivity of their cargo may not be affected much. Whether the modified exosomes maintain the basic characteristics of natural exosomes like low immunogenicity should be evaluated in the future. In the other hand, the size of exosomes was increased and heterogeneous after the modification and gradient purification. But the cRGD-Exo still presented intact vesicle shape and no further aggregation, and showed targeting ability and therapeutic efficacy *in vivo*.

After intravenous administration to mice receiving MCAO/R, cRGD-Exo significantly accumulated in the lesion region of the ischemic brain. Our results suggest that the targeting capability of cRGD-Exo was mediated by recognition of integrin $\alpha_v\beta_3$, where its expression on cerebral vascular endothelial cells is induced by ischemia. Earlier studies reported that RGD-modified nanoparticles accumulate around blood vessels and cannot readily penetrate into the parenchyma [58]. However, our data verify that the cRGD-Exo efficiently entered microglia, neurons, and astrocytes. In fact, as a natural transporter, exosomes can cross biological barriers more efficiently than nanoparticles and liposomes [13,59]. Previous reports have suggested that bioactive proteins on the exosome surface may mediate exosome delivery into the brain parenchyma *via* transcytosis [60]. In addition, although the BBB is damaged, it is one of the biggest obstacles for drug delivery in stroke [5]. In the model of MCAO, a biphasic opening of the BBB was evoked at 5 and 72 h of reperfusion respectively [61,62]. Our images of brain slices showed that exosomes were entrapped in brain cells upon intravenous administration 12 h after reperfusion, suggesting that exosomes cross the BBB to a certain extent.

Based on our data, intravenously administered cRGD-Exo-cur, which is an acceptable route of administration, effectively suppressed inflammation and cellular apoptosis in the lesion region of the ischemic brain. According to preclinical studies, anti-inflammatory treatment provided unique advantages, such as could be applied to treat patients after the time window for thrombolysis [45]. Furthermore, cRGD-Exo acted as an effective curcumin delivery vehicle for cerebral ischemia therapy in this work. Other therapeutic agents could be loaded onto cRGD-Exo for targeted delivery to the lesion region of the ischemic brain in the further. Many effective loading strategies including the engineering of producer cells [21,22], electroporation [20], sonication [63], passive incubation with permeabilization agents [63], and incubation with hydrophobically modified RNAs [64] have been developed to load small therapeutic molecules, RNAs (siRNAs and miRNAs), and even proteins onto exosomes. Thus, exosomes could be an effective complement to synthetic carriers especially when they fail by immune responses, toxicity, or BBB isolation. One possible problem may be the accumulation of cRGD-Exo in the liver and lungs resulting from high levels of integrin $\alpha_v\beta_3$ in the liver and the size of cRGD-Exo [43]. Neither tissue damage nor function loss was observed on the liver and lungs after the intravenous administration of exosomes [65,66], however, the liver and lung toxicity of the drugs loaded into exosomes should be well evaluated before clinic application. Here we have confirmed the safety of cRGD-Exo-cur treatment.

Because c(RGDyK) is a well-known tumor-targeting ligand [41], future studies may explore drug delivery to tumors by cRGD-Exo. Also, the beneficial effects of exosomes have been revealed in different studies such as ischemic heart injury [67,68] and acute kidney injury [69]. Based on our method, exosomes or EVs could be modified with other moieties, including peptides, nanobodies, PEG derivatives, and molecular probes, and the moiety densities could be optimized to satisfy different applications. To increase the yield of exosomes, conditioned medium from stem cell industry can be a stable source, and an immortalized MSC cell line could be used instead of primary cells [70]. Alternatively, a sufficient number of safe exosomes can be isolated from the blood [71]. We believe that this biochemical engineering method is suitable for large-scale production of functionalized exosomes within a short duration, which would allow exosomes to be utilized as drug vehicles for clinical applications in different fields.

Author contributions

J.G. and T.T. designed the study. T.T. performed most experimental work and analyses. H.-X.Z. contributed animal model. C.-P.H., S.F., Y.-L.Z. and C.Q. provided assistance. N.-P.H., Z.-D.X. Z.-H.L. and B.A.T. contributed technical supports and discussion. T.T., B.A.T. and J.G. wrote/edited the manuscript.

Acknowledgements

This work was supported by grants from the National Natural Science Foundation of China (No. 81222013, 81673416) and Key R&D program of Jiangsu Province (No. BE2016761) to J. Gao, the National Natural Science Foundation of China (No. 81401092) and the Natural Science Foundation of Jiangsu Province (No. BK20170107, BK20130886) to T. Tian. We thank Wen-Tao Liu (Nanjing Medical University, Nanjing, China) and Cong Li (Fudan University, Shanghai, China) for critical reading of the manuscript.

Appendix A. Supplementary data

Supplementary data related to this article can be found at https://doi.org/10.1016/j.biomaterials.2017.10.012.

Competing financial interests

Tian Tian and Jun Gao have filed a patent application on the method of the chemical modification on exosome surface.

References

[1] P.J. Kelly, E. Kavanagh, S. Murphy, Stroke, New developments and their application in clinical practice, Semin. Neurol. 36 (2016) 317–323.
[2] D. Mozaffarian, E.J. Benjamin, A.S. Go, D.K. Arnett, M.J. Blaha, M. Cushman, et al., Heart disease and stroke Statistics-2016 update: a report from the american heart association, Circulation 133 (2016) e38–360.
[3] J. Rother, G.A. Ford, V.N. Thijs, Thrombolytics in acute ischaemic stroke: historical perspective and future opportunities, Cerebrovasc. Dis. 35 (2013) 313–319.
[4] M. Fisher, J.L. Saver, Future directions of acute ischaemic stroke therapy, Lancet Neurol. 14 (2015) 758–767.
[5] T. Rhim, D.Y. Lee, M. Lee, Drug delivery systems for the treatment of ischemic stroke, Pharm. Res. 30 (2013) 2429–2444.
[6] B.J. Thompson, P.T. Ronaldson, Drug delivery to the ischemic brain, Adv. Pharmacol. 71 (2014) 165–202.
[7] R. Kalluri, The biology and function of exosomes in cancer, J. Clin. Invest 126 (2016) 1208–1215.
[8] M. Tkach, C. Théry, Communication by extracellular vesicles: where we are and where we need to go, Cell 164 (2016) 1226–1232.
[9] M. Simons, G. Raposo, Exosomes–vesicular carriers for intercellular communication, Curr. Opin. Cell Biol. 21 (2009) 575–581.
[10] J.M. Pitt, G. Kroemer, L. Zitvogel, Extracellular vesicles: masters of intercellular communication and potential clinical interventions, J. Clin. Invest 126 (2016) 1139–1143.
[11] T. Lener, M. Gimona, L. Aigner, V. Borger, E. Buzas, G. Camussi, et al., Applying extracellular vesicles based therapeutics in clinical trials - an ISEV position paper, J. Extracell. Vesicles 4 (2015) 30087.
[12] S. Fais, L. O'Driscoll, F.E. Borras, E. Buzas, G. Camussi, F. Cappello, et al., Evidence-based clinical use of nanoscale extracellular vesicles in nanomedicine, ACS Nano 10 (2016) 3886–3899.
[13] S. El Andaloussi, S. Lakhal, I. Mager, M.J. Wood, Exosomes for targeted siRNA delivery across biological barriers, Adv. Drug Deliv. Rev. 65 (2013) 391–397.
[14] P. Vader, E.A. Mol, G. Pasterkamp, R.M. Schiffelers, Extracellular vesicles for drug delivery, Adv. Drug Deliv. Rev. 106 (2016) 148–156.
[15] D. Ingato, J.U. Lee, S.J. Sim, Y.J. Kwon, Good things come in small packages: overcoming challenges to harness extracellular vesicles for therapeutic delivery, J. Control Release 241 (2016) 174–185.
[16] S.A. Kooijmans, R.M. Schiffelers, N. Zarovni, R. Vago, Modulation of tissue tropism and biological activity of exosomes and other extracellular vesicles: new nanotools for cancer treatment, Pharmacol. Res. 111 (2016) 487–500.
[17] C.P. Lai, O. Mardini, M. Ericsson, S. Prabhakar, C.A. Maguire, J.W. Chen, et al., Dynamic biodistribution of extracellular vesicles in vivo using a multimodal imaging reporter, ACS Nano 8 (2014) 483–494.
[18] O.P. Wiklander, J.Z. Nordin, A. O'Loughlin, Y. Gustafsson, G. Corso, I. Mager, et al., Extracellular vesicle in vivo biodistribution is determined by cell source, route of administration and targeting, J. Extracell. Vesicles 4 (2015) 26316.
[19] J.P. Armstrong, M.N. Holme, M.M. Stevens, Re-engineering extracellular vesicles as smart nanoscale therapeutics, ACS Nano 11 (2017) 69–83.
[20] L. Alvarez-Erviti, Y. Seow, H. Yin, C. Betts, S. Lakhal, M.J. Wood, Delivery of siRNA to the mouse brain by systemic injection of targeted exosomes, Nat. Biotechnol. 29 (2011) 341–345.
[21] Y. Liu, D. Li, Z. Liu, Y. Zhou, D. Chu, X. Li, et al., Targeted exosome-mediated delivery of opioid receptor Mu siRNA for the treatment of morphine relapse, Sci. Rep. 5 (2015) 17543.
[22] S. Ohno, M. Takanashi, K. Sudo, S. Ueda, A. Ishikawa, N. Matsuyama, et al., Systemically injected exosomes targeted to EGFR deliver antitumor microRNA to breast cancer cells, Mol. Ther. 21 (2013) 185–191.
[23] S.A. Kooijmans, L.A. Fliervoet, R. van der Meel, M.H. Fens, H.F. Heijnen, P.M. van Bergen En Henegouwen, et al., PEGylated and targeted extracellular vesicles display enhanced cell specificity and circulation time, J. Control Release 224 (2016) 77–85.
[24] T. Smyth, K. Petrova, N.M. Payton, I. Persaud, J.S. Redzic, M.W. Graner, et al., Surface functionalization of exosomes using click chemistry, Bioconjug. Chem. 25 (2014) 1777–1784.
[25] Y.T. Sato, K. Umezaki, S. Sawada, S.A. Mukai, Y. Sasaki, N. Harada, et al., Engineering hybrid exosomes by membrane fusion with liposomes, Sci. Rep. 6 (2016) 21933.
[26] T. Abumiya, J. Lucero, J.H. Heo, M. Tagaya, J.A. Koziol, B.R. Copeland, et al., Activated microvessels express vascular endothelial growth factor and integrin alpha(v)beta3 during focal cerebral ischemia, J. Cereb. Blood Flow. Metab. 19 (1999) 1038–1050.
[27] K. Guell, G.J. Bix, Brain endothelial cell specific integrins and ischemic stroke, Expert Rev. Neurother. 14 (2014) 1287–1292.
[28] R. Haubner, H.J. Wester, F. Burkhart, R. Senekowitsch-Schmidtke, W. Weber, S.L. Goodman, et al., Glycosylated RGD-containing peptides: tracer for tumor targeting and angiogenesis imaging with improved biokinetics, J. Nucl. Med. 42 (2001) 326–336.
[29] D. Arosio, C. Casagrande, Advancement in integrin facilitated drug delivery, Adv. Drug Deliv. Rev. 97 (2016) 111–143.
[30] C. Théry, S. Amigorena, G. Raposo, A. Clayton, Isolation and characterization of exosomes from cell culture supernatants and biological fluids, Curr. Protoc. Cell Biol. Chapter 3 (2006). Unit 3 22.
[31] D.Y. Zhu, Q. Deng, H.H. Yao, D.C. Wang, Y. Deng, G.Q. Liu, Inducible nitric oxide synthase expression in the ischemic core and penumbra after transient focal cerebral ischemia in mice, Life Sci. 71 (2002) 1985–1996.
[32] S. Ashwal, B. Tone, H.R. Tian, D.J. Cole, W.J. Pearce, Core and penumbral nitric oxide synthase activity during cerebral ischemia and reperfusion, Stroke 29 (1998) 1037–1046.
[33] E.J. van der Vlist, E.N. Nolte-'t Hoen, W. Stoorvogel, G.J. Arkesteijn, M.H. Wauben, Fluorescent labeling of nano-sized vesicles released by cells and subsequent quantitative and qualitative analysis by high-resolution flow cytometry, Nat. Protoc. 7 (2012) 1311–1326.
[34] D. Sun, X. Zhuang, X. Xiang, Y. Liu, S. Zhang, C. Liu, et al., A novel nanoparticle drug delivery system: the anti-inflammatory activity of curcumin is enhanced when encapsulated in exosomes, Mol. Ther. 18 (2010) 1606–1614.
[35] D.L. Rupert, V. Claudio, C. Lasser, M. Bally, Methods for the physical characterization and quantification of extracellular vesicles in biological samples, Biochim. Biophys. Acta 1861 (2017) 3164–3179.
[36] T. Teklemariam, A.I. Seoane, C.J. Ramos, E.E. Sanchez, S.E. Lucena, J.C. Perez, et al., Functional analysis of a recombinant PIII-SVMP, GST-acocostatin; an apoptotic inducer of HUVEC and HeLa, but not SK-Mel-28 cells, Toxicon 57 (2011) 646–656.
[37] X. Liu, W. Wang, D. Samarsky, L. Liu, Q. Xu, W. Zhang, et al., Tumor-targeted in vivo gene silencing via systemic delivery of cRGD-conjugated siRNA, Nucleic Acids Res. 42 (2014) 11805–11817.
[38] S. Monferran, N. Skuli, C. Delmas, G. Favre, J. Bonnet, E. Cohen-Jonathan-Moyal, et al., Alphavbeta3 and alphavbeta5 integrins control glioma cell response to ionising radiation through ILK and RhoB, Int. J. Cancer 123 (2008) 357–364.
[39] H. Memezawa, M.L. Smith, B.K. Siesjo, Penumbral tissues salvaged by reperfusion following middle cerebral artery occlusion in rats, Stroke 23 (1992) 552–559.
[40] L. Li, F. Liu, J.V. Welser-Alves, L.D. McCullough, R. Milner, Upregulation of fibronectin and the alpha5beta1 and alphavbeta3 integrins on blood vessels within the cerebral ischemic penumbra, Exp. Neurol. 233 (2012) 283–291.
[41] Q. Chen, X. Wang, C. Wang, L. Feng, Y. Li, Z. Liu, Drug-induced self-assembly of modified albumins as nano-theranostics for tumor-targeted combination therapy, ACS Nano 9 (2015) 5223–5233.
[42] A.J. Shuhendler, P. Prasad, M. Leung, A.M. Rauth, R.S. Dacosta, X.Y. Wu, A novel solid lipid nanoparticle formulation for active targeting to tumor alpha(v) beta(3) integrin receptors reveals cyclic RGD as a double-edged sword, Adv. Healthc. Mater. 1 (2012) 600–608.
[43] Y. Zheng, S. Ji, E. Tomaselli, Y. Yang, S. Liu, Comparison of biological properties of (111)In-labeled dimeric cyclic RGD peptides, Nucl. Med. Biol. 42 (2015) 137–145.
[44] J.H. Liu, S.T. Yang, H. Wang, Y. Chang, A. Cao, Y. Liu, Effect of size and dose on the biodistribution of graphene oxide in mice, Nanomedicine (Lond) 7 (2012) 1801–1812.
[45] C. Iadecola, J. Anrather, The immunology of stroke: from mechanisms to translation, Nat. Med. 17 (2011) 796–808.
[46] R. Milner, Microglial expression of alphavbeta3 and alphavbeta5 integrins is regulated by cytokines and the extracellular matrix: beta5 integrin null microglia show no defects in adhesion or MMP-9 expression on vitronectin, Glia 57 (2009) 714–723.
[47] Y. Zhang, M. Chopp, X.S. Liu, M. Katakowski, X. Wang, X. Tian, et al., Exosomes derived from mesenchymal stromal cells promote axonal growth of cortical neurons, Mol. Neurobiol. 54 (2017) 2659–2673.
[48] A. Kalani, P.K. Kamat, K. Kalani, N. Tyagi, Epigenetic impact of curcumin on stroke prevention, Metab. Brain Dis. 30 (2015) 427–435.
[49] T. Chang, D. Trench, J. Putnam, M.H. Stenzel, M.S. Lord, Curcumin-loading-dependent stability of PEGMEMA-based micelles affects endocytosis and exocytosis in colon carcinoma cells, Mol. Pharm. 13 (2016) 924–932.
[50] S.E. Lakhan, A. Kirchgessner, M. Hofer, Inflammatory mechanisms in ischemic stroke: therapeutic approaches, J. Transl. Med. 7 (2009) 97.
[51] K.L. Lambertsen, K. Biber, B. Finsen, Inflammatory cytokines in experimental and human stroke, J. Cereb. Blood Flow. Metab. 32 (2012) 1677–1698.
[52] Y. Zhang, M. Chopp, Z.G. Zhang, M. Katakowski, H. Xin, C. Qu, et al., Systemic administration of cell-free exosomes generated by human bone marrow derived mesenchymal stem cells cultured under 2D and 3D conditions improves functional recovery in rats after traumatic brain injury, Neurochem. Int. (2016), https://doi.org/10.1016/j.neuint.2016.08.003 pii: S0197-0186(16)30251-0.
[53] B. Zhang, Y. Yin, R.C. Lai, S.S. Tan, A.B. Choo, S.K. Lim, Mesenchymal stem cells secrete immunologically active exosomes, Stem Cells Dev. 23 (2014) 1233–1244.
[54] X.K. Tu, W.Z. Yang, J.P. Chen, Y. Chen, L.Q. Ouyang, Y.C. Xu, et al., Curcumin inhibits TLR2/4-NF-kappaB signaling pathway and attenuates brain damage in permanent focal cerebral ischemia in rats, Inflammation 37 (2014) 1544–1551.
[55] S.T. Laughlin, J.M. Baskin, S.L. Amacher, C.R. Bertozzi, In vivo imaging of membrane-associated glycans in developing zebrafish, Science 320 (2008) 664–667.
[56] J.M. Baskin, J.A. Prescher, S.T. Laughlin, N.J. Agard, P.V. Chang, I.A. Miller, et al., Copper-free click chemistry for dynamic in vivo imaging, Proc. Natl. Acad. Sci. U. S. A. 104 (2007) 16793–16797.
[57] H. Koo, S. Lee, J.H. Na, S.H. Kim, S.K. Hahn, K. Choi, et al., Bioorthogonal copper-free click chemistry in vivo for tumor-targeted delivery of nanoparticles, Angew. Chem. Int. Ed. Engl. 51 (2012) 11836–11840.

[58] K.N. Sugahara, T. Teesalu, P.P. Karmali, V.R. Kotamraju, L. Agemy, O.M. Girard, et al., Tissue-penetrating delivery of compounds and nanoparticles into tumors, Cancer Cell 16 (2009) 510–520.
[59] A. Aryani, B. Denecke, Exosomes as a nanodelivery system: a Key to the future of neuromedicine? Mol. Neurobiol. 53 (2016) 818–834.
[60] M. Grapp, A. Wrede, M. Schweizer, S. Huwel, H.J. Galla, N. Snaidero, et al., Choroid plexus transcytosis and exosome shuttling deliver folate into brain parenchyma, Nat. Commun. 4 (2013) 2123.
[61] K.E. Sandoval, K.A. Witt, Blood-brain barrier tight junction permeability and ischemic stroke, Neurobiol. Dis. 32 (2008) 200–219.
[62] S. Engelhardt, S. Patkar, O.O. Ogunshola, Cell-specific blood-brain barrier regulation in health and disease: a focus on hypoxia, Br. J. Pharmacol. 171 (2014) 1210–1230.
[63] M.J. Haney, N.L. Klyachko, Y. Zhao, R. Gupta, E.G. Plotnikova, Z. He, et al., Exosomes as drug delivery vehicles for Parkinson's disease therapy, J. Control Release 207 (2015) 18–30.
[64] M.C. Didiot, L.M. Hall, A.H. Coles, R.A. Haraszti, B.M. Godinho, K. Chase, et al., Exosome-mediated delivery of hydrophobically modified siRNA for huntingtin mRNA silencing, Mol. Ther. 24 (2016) 1836–1847.
[65] S. Kamerkar, V.S. LeBleu, H. Sugimoto, S. Yang, C.F. Ruivo, S.A. Melo, et al., Exosomes facilitate therapeutic targeting of oncogenic KRAS in pancreatic cancer, Nature 546 (2017) 498–503.
[66] L. Sun, R. Xu, X. Sun, Y. Duan, Y. Han, Y. Zhao, et al., Safety evaluation of exosomes derived from human umbilical cord mesenchymal stromal cell, Cytotherapy 18 (2016) 413–422.
[67] S. Sahoo, D.W. Losordo, Exosomes and cardiac repair after myocardial infarction, Circ. Res. 114 (2014) 333–344.
[68] Z.A. Malik, K.S. Kott, A.J. Poe, T. Kuo, L. Chen, K.W. Ferrara, et al., Cardiac myocyte exosomes: stability, HSP60, and proteomics, Am. J. Physiol. Heart Circ. Physiol. 304 (2013) H954–H965.
[69] C. Grange, M. Tapparo, S. Bruno, D. Chatterjee, P.J. Quesenberry, C. Tetta, et al., Biodistribution of mesenchymal stem cell-derived extracellular vesicles in a model of acute kidney injury monitored by optical imaging, Int. J. Mol. Med. 33 (2014) 1055–1063.
[70] R.W. Yeo, R.C. Lai, B. Zhang, S.S. Tan, Y. Yin, B.J. Teh, et al., Mesenchymal stem cell: an efficient mass producer of exosomes for drug delivery, Adv. Drug Deliv. Rev. 65 (2013) 336–341.
[71] H. Qi, C. Liu, L. Long, Y. Ren, S. Zhang, X. Chang, et al., Blood exosomes endowed with magnetic and targeting properties for cancer therapy, ACS Nano 10 (2016) 3323–3333.